Optics & Laser Technology 188 (2025) 112919

Contents lists available at ScienceDirect

Optics and Laser Technology

journal homepage: www.elsevier.com/locate/optlastec

Full length article

Ultrahigh sensitive liquid core fiber Mach–Zehnder interferometer using a low light absorption

Cheng-Ling Lee [a,*], Jen-Te Chao [a], Ying-Zhen Huang [a], Yi-Hua Wu [a], Yi-Kai Chiu [a], Wei-Wei Hsiang [b]

[a] Department of Electro-Optical Engineering, National United University, Miaoli City 360, Taiwan
[b] Department of Physics, Fu Jen Catholic University, New Taipei City 242, Taiwan

ARTICLE INFO

Keywords:
Liquid-core fiber Mach–Zehnder interferometer (LCFMZI)
Hollow-core fiber (HCF)
Laser diode (LD)
Light absorption
Liquid

ABSTRACT

This paper presents an advanced liquid-core fiber Mach–Zehnder interferometer (LCFMZI) designed to have the ultra-low light absorption properties of the liquid core for achieving ultrasensitive spectral responses. The device structure features a micro-sized hollow-core fiber (HCF) with a core diameter of 10 μm, spliced between two single-mode fibers (SMFs) with tilted ends. This configuration minimizes Fresnel reflections and creates a miniature oblique gap for liquid filling. The interference mechanism is based on the superposition of core and cladding modes, with a 5 μm core offset strategically introduced to enhance mode coupling and achieve a high extinction ratio in the output interference spectra. When irradiated by a 980 nm laser diode (LD), the liquid core, serving as an absorber, undergoes a temperature-induced refractive index (RI) change, which alters the optical path difference in the LCFMZI. This results in a substantial wavelength shift in the interference pattern. Experimental results demonstrate remarkable spectral shifts of over 124 nm over the broadband range of 1250–1650 nm with an LD input power as low as 0.566 mW. The proposed LCFMZI achieves an exceptional sensitivity of + 219.08 nm/mW and 3.647 nm/mA with a highly linear response. A theoretical analysis was also performed, demonstrating good agreement with the experimental results. These results validate the effectiveness of the LCFMZI's low light absorption mechanism in achieving ultrahigh sensitivity.

1. Introduction

All-fiber optic sensors offer significant advantages, such as high sensitivity, compactness, resistance to harsh environments, and multiplexing capabilities, driving their rapid adoption in fields like environmental monitoring, structural health assessment, biomedical diagnostics, and industrial automation. Among these fiber optic sensors, fiber Mach-Zehnder interferometer (FMZI) is particularly attractive because they are simply operated in a transmission system, and are highly sensitive. The principle of interference is where an input light signal is split into two paths, one of which interacts with the external environment, before being recombined to produce interference patterns. External factors such as temperature (T), strain (ε), pressure (P), and refractive index (RI) variations induce wavelength shifts in the interference spectra, enabling precise measurements of these parameters. This makes FMZIs ideal for real-time, remote, and high-sensitivity multi-parameter sensing in advanced technologies.

Numerous configurations for the FMZIs have been proposed in the literature and have demonstrated their effectiveness. An offset fusion method is generally used to achieve two paths of light for better interference in many FMZI configurations. An FMZI using large offset fusion has been shown to exhibit high sensitivity in gas refractive index (RI) measurements [1], an SMF's RI sensor based on the core offset attenuators [2], and an arc-fused small lateral offset fiber sensor has shown its remarkable sensing capabilities[3]. Another configuration that uses thin-core fiber to cause light splitting has been reported. An RI sensor based on transmission and reflection thin-core fiber modes has also demonstrated excellent performance [4]. An in-line Mach-Zehnder interferometer using thin-core fiber for ammonia gas sensing with high sensitivity has been presented in [5]. High-performance optical fiber sensors employing immersed-oriented liquid crystals have demonstrated their effectiveness [6]. When a standard optical fiber is spliced with a D-shaped fiber to form an FMZI, its asymmetric structure creates a path difference at the section where it is located [7]. A liquid core fiber

* Corresponding author.
E-mail address: cherry@nuu.edu.tw (C.-L. Lee).

https://doi.org/10.1016/j.optlastec.2025.112919
Received 16 January 2025; Received in revised form 9 March 2025; Accepted 31 March 2025

interferometer for simultaneous measurement of RI and T has been proposed. Unfortunately, the filled liquid would disappear and be challenging to retain due to the fiber fusion splicing process [8]. Therefore, SMF-microfiber-SMF structures have been used to achieve high sensitivity with liquid-assisted cooperation to assist filled liquid over the microfiber section for forming the FMZIs [9,10]. After that, FMZI sensors fabricated by femtosecond laser micromachining on SMF [11], microstructured optical fiber (MOF) [12], and hollow-core fiber (HCF) [13] have demonstrated their advancement in the measurement with liquid and gas, respectively. It indicates that the structure of optical fibers with microholes allows for the infusion of materials, making it more flexible to combine other materials with a high thermal expansion coefficient and a high thermo-optic coefficient, enabling the achievement of high sensitivity of measurement [14]. Moreover, it is particularly advantageous for measuring precious and rare materials, requiring only a picoliter volume. An FMZI is fabricated by selectively filling liquid into one air hole of the innermost layer of a photonic crystal fiber (PCF). Due to the high thermo-optic coefficient (TOC) of the liquid, interference modes can be significantly modified to obtain extreme variations of the optical spectra. The only drawback is that after infusing liquids into microholes, the PCF and SMF cannot be directly fusion spliced; instead, the direct manual gluing method must be used, which may result in a less stable configuration [15]. The sizeable lateral offset and open-cavity structure provide excellent RI sensing sensitivity (−13,703.63 nm/RIU) and are optimized for seawater monitoring, making them highly suitable for applications in marine science and environmental monitoring. However, their application range is relatively narrow (1.3370–1.3410), and the open-cavity structure makes the sensor more susceptible to environmental influences [16]. The piecewise interference spectrum was proposed to mark the interference valley positions and was tested using a glycerol aqueous solution for refractive index measurement. However, due to the eccentric-hole dual-core structure, fabrication is more challenging and requires precise fusion of dual-core optical fibers [17]. To overcome the limitation of direct fusion splicing after liquid infusion, Lee et al. proposed an ultracompact, leaky-guided liquid-core FMZI. This design employs a micro-sized HCF spliced to tilted-end SMFs, forming a miniature oblique gap for liquid infusion [18].

In this study, we advance designing an ultrasensitive FMZI with inherently slight laser light absorption at a wavelength of 980 nm in the liquid core. The LCFMZI incorporates a tilted and offset core configuration between the SMF and the HCF to create a microchannel, facilitating rapid liquid filling in approximately 5.3 s. Using Cargille liquid with an RI of $n_D = 1.46$ [19], the liquid core maintains fiber waveguide transmission properties, and the liquid's high thermo-optic coefficient (TOC) significantly modulates the fiber core mode. In contrast to previous studies, such as [9], where light-responsive liquids were exposed in an open configuration with external laser excitation, our work integrates the laser light directly into the liquid-filled core of the fiber waveguide. When irradiated with a 980 nm laser diode (LD), the filled liquid absorbs the light, inducing a temperature (T) rise that alters its RI, thereby modifying the optical path difference in the LCFMZI to vary the optical interference spectra. Experimental results demonstrate a 124 nm spectral shift across a broadband wavelength range of 1250–1650 nm with a 980 nm LD power as low as 0.566 mW, or even lower, due to the imperfect alignment of the core offset in the waveguide structure. A sensitivity of + 219.08 nm/mW and 3.647 nm/mA with the linear response ($r^2 = 0.9993$), validating the proposed LCFMZI's effectiveness in achieving ultrahigh sensitivity controlled by a low light absorption.

2. LCFMZI fabrication and Operating principle

The LCFMZI fabrication flowchart is displayed in Fig. 1. First, we use a fiber cleaver to create flat end faces on both sides of a section of HCF with a length of approach 1 cm. The HCF has an inner core diameter of 10 μm and an outer cladding diameter of 125 μm. Next, slant-cleaving techniques are applied to the SMF endfaces using a Fujikura CT-100 fiber cleaver, followed by biased fusion splicing to the HCF with a 5 μm core offset using a Fujikura FSM-90 s fusion splicer. The process creates a tiny gap between the HCF and SMF. Similarly, the other end of the HCF is spliced with an obliquely cleaved SMF, forming a symmetrical structure that facilitates liquid filling, as illustrated in Fig. 1(a)–(c). A micrograph of the fabricated device is shown in Fig. 1(d). Following this, we fill the device with Cargille-liquid with an RI of $n_D = 1.46$ via capillarity. The filling process is depicted in Fig. 1(e) to (g). In the filling step, we employ a custom-designed holder with a central V-groove, allowing the device to remain slightly suspended during encapsulation. When one open end of the tiny gap encounters the liquid drop, capillary

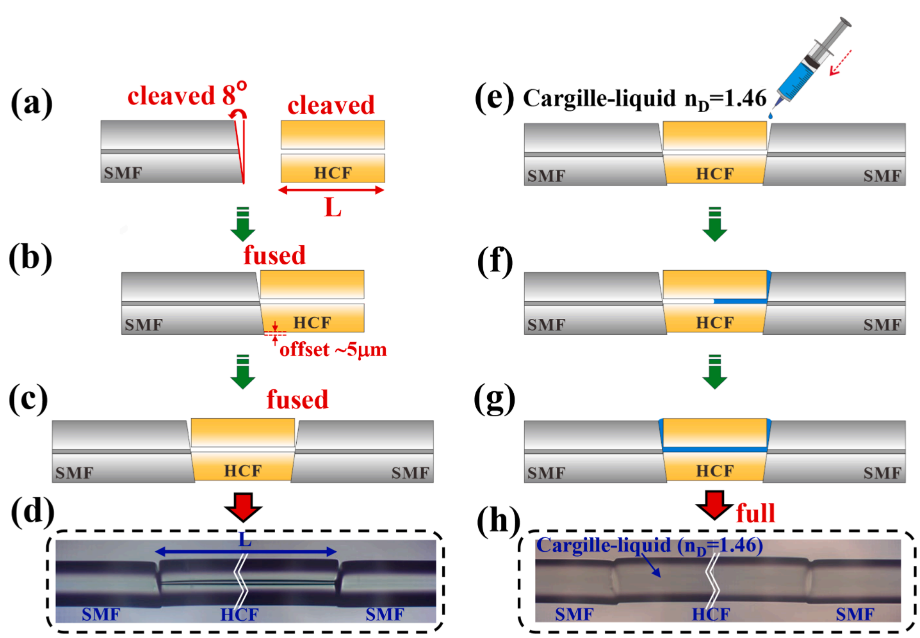

Fig. 1. (a)-(c) The fabrication flow chart for the proposed device. (e)-(g) Schematic evolutions of the device for infusing with Cargille liquid ($n_D = 1.46$). (d) and (h) are the microphotographs that are non-filled and filled with the liquid.

action drives spontaneous liquid transport through the hollow core toward the opposite open end, ensuring uniform filling without needing external force-driven methods. The entire capillary filling process has been observed under a microscope to monitor its behavior in real time. An open, unobstructed exit at the opposite end generally allows continuous liquid flow and prevents trapped air bubbles. Finally, the microscopic photographs of the non-filled and filled liquids are shown in Fig. 1(d) and Fig. 1 (h), respectively.

To better understand the interference mechanism of the LCFMZI, we conducted theoretical simulations of the fiber waveguide structure. In the calculation, the liquid core and cladding diameters of the LCFMZI are set to be 10 μm and 125 μm, respectively, and their RIs curves of liquid core $N_{co}(\lambda)$ and fiber cladding $N_{cl}(\lambda)$ are based on the dispersion equations of the as shown in [20] and [21], respectively. The calculated refractive index (RI) based on the following equations $N_{co}(\lambda) = 1.447925+\frac{4.073\times10^{-3}}{\lambda^2} + \frac{4.1636939\times10^{-5}}{\lambda^4}$($\lambda$ in μm) and, $N_{cl}(\lambda)$ $\sqrt{1+\frac{0.6961663\lambda^2}{\lambda^2-0.004679148}+\frac{0.4079426\lambda^2}{\lambda^2-0.01351206}+\frac{0.8974794\lambda^2}{\lambda^2-97.934002}}=$ (λ in μm), respectively. The Ris of the liquid core and the fiber cladding at 25 °C are plotted in Fig. 2(a). The effective index of the core and cladding modes can be obtained by further calculating the proposed fiber waveguide with the dispersion equations of the LP modes, which is expressed as follows [22]:

$$\frac{J_n(u)}{uJ_{n-1}(u)} = -\frac{K_n(w)}{wK_{n-1}(w)} \tag{1}$$

The above Eq. (1) is utilized to derive the relationships between the effective index of the liquid core mode and the cladding modes, as shown in Fig. 2(b). n denotes the azimuthal mode number. The Bessel function formulas $J_{-1}(u) = -J_1(u)$ and $K_{-1}(w) = K_1(w)$ are applied to Eq. (1) for the LP_{01} mode (n = 0), for the LP_{11} modes (n = 1), the same dispersion equation is approximately satisfied.

Here, the parameters u and w are defined as $u = a\sqrt{\left(k^2\times N_{co}^2\right)-\beta^2}$; $w = a\sqrt{\beta^2-(k^2\times N_{cl}^2)}$, k represents the wave number, β is the propagation constant, and β= $k\,Neff$, and a = 5 μm is the liquid core radius. The N_{eff}^{co} and N_{eff}^{cl} denote the effective indices of the core and cladding modes, respectively. The Bessel function relationships facilitate the analysis of propagation mode characteristics in the liquid core fiber waveguide.

Here, the effective indices for the liquid core modes of LP_{01}, and LP_{11} and the first five-order cladding modes are displayed, and they are denoted as $N_{eff-LP01}^{co}$, $N_{eff-LP11}^{co}$ and $N_{eff}^{cl,m=1-5}$, respectively. The obtained results will significantly benefit our subsequent analysis of the transmission interference spectrum in the proposed LCFMZI, providing a precise means of interference measurement and spectral control in the proposed optical fiber waveguide.

The interference mechanism of the proposed LCFMZI is primarily based on the superposition of the core mode(N_{eff}^{co}) and the m-th order cladding mode ($N_{eff}^{cl,m}$). In this structure, the interference occurs as these modes propagate through the hollow-core fiber (HCF) with a length L. The optical phase difference (ϕ_m) between the core mode and the m-th order cladding mode is expressed as:

$$\phi_m = \frac{2\pi}{\lambda}\left(N_{eff}^{co}-N_{eff}^{cl,m}\right)L = \frac{2\pi}{\lambda}\Delta N_{eff}^{m}L \tag{2}$$

Here, λ represents the wavelength of light in a vacuum, and ΔN_{eff}^{m} is the effective index difference between the core mode and the m-th order cladding mode ($\Delta N_{eff}^{m} = N_{eff}^{co} - N_{eff}^{cl,m}$). The optical path difference (OPD) is denoted as $\Delta N_{eff}^{m}L$. Variations in the effective index difference (ΔN_{eff}^{m}) influence both the phase difference and the wavelengths that satisfy the interference conditions. As a result, the spectral position of interference peaks and dips shifts correspondingly. For constructive interference (ϕ_m = 2pπ), the wavelength of maximum output power (λ_{max}^{m}) can be determined. The values of effective index difference ΔN_{eff}^{m} for constructive interference can be expressed in terms of the interference order p (positive integer):

$$\Delta N_{eff}^{m} = \frac{p\times\lambda_{max}^{m}}{L} \tag{3}$$

By substituting the interference orders (p = 3 to 8) into Eq. (3), the measured wavelengths from 1250 nm to 1650 nm are used to match the calculated ΔN_{eff}^{m}. The actual interference length is measured as L = 0.92 cm. The values of $\frac{p\times\lambda_{max}^{m}}{L}$ over this wavelength range are depicted as rainbow-colored lines in Fig. 3(a). On the other hand, the black line in Fig. 3(a) represents $\Delta N_{eff}^{m=1}$ (for coupling m = 1 cladding mode), which is derived from the difference between $N_{eff-LP11}^{co}$ and $N_{eff}^{cl,m=1}$ in Fig. 2(b). We can see from the results that the range of the interference order (p) that intersects with the ΔN_{eff}^{m} in the measured wavelength band can be observed. The black line $\Delta N_{eff}^{m=1}$, whose intersections with different interference orders of p, represent correspondingly the wavelengths of the constructive interference peaks λ_{max}^{m} with orders of p = 3 to 8. Based on the intersections in Fig. 3(a) and the experimental result shown in Fig. 3(b), agreements are found to confirm the effectiveness of the proposed model. Comparing the wavelengths of the interference peaks of interference spectra by theoretical simulation from Fig. 3(a) and the experimental transmission spectrum reveals six resonance peaks in the

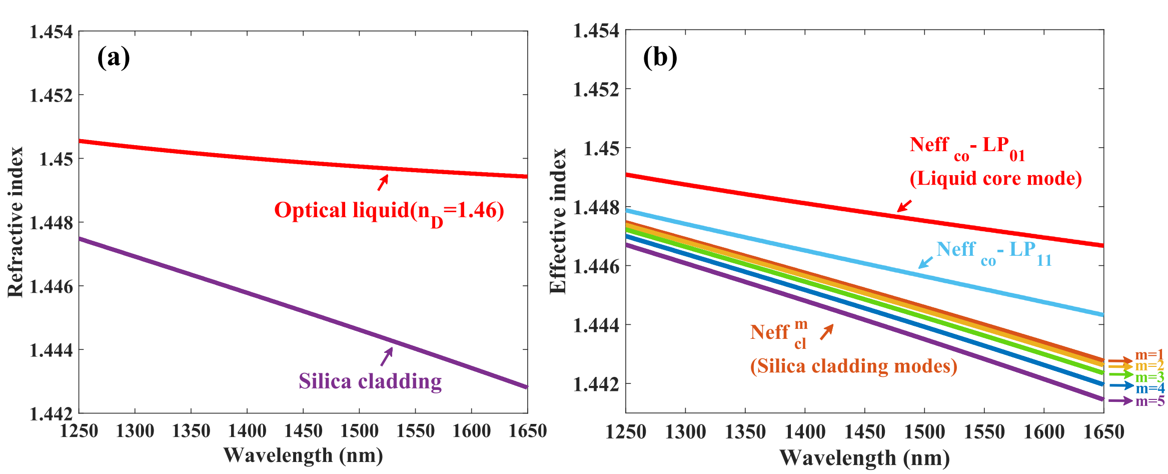

Fig. 2. (a) Refractive index dispersions of the used liquid and silica cladding. (b) The effective index of the core mode and the first 5th-order cladding modes in the proposed waveguide structure.

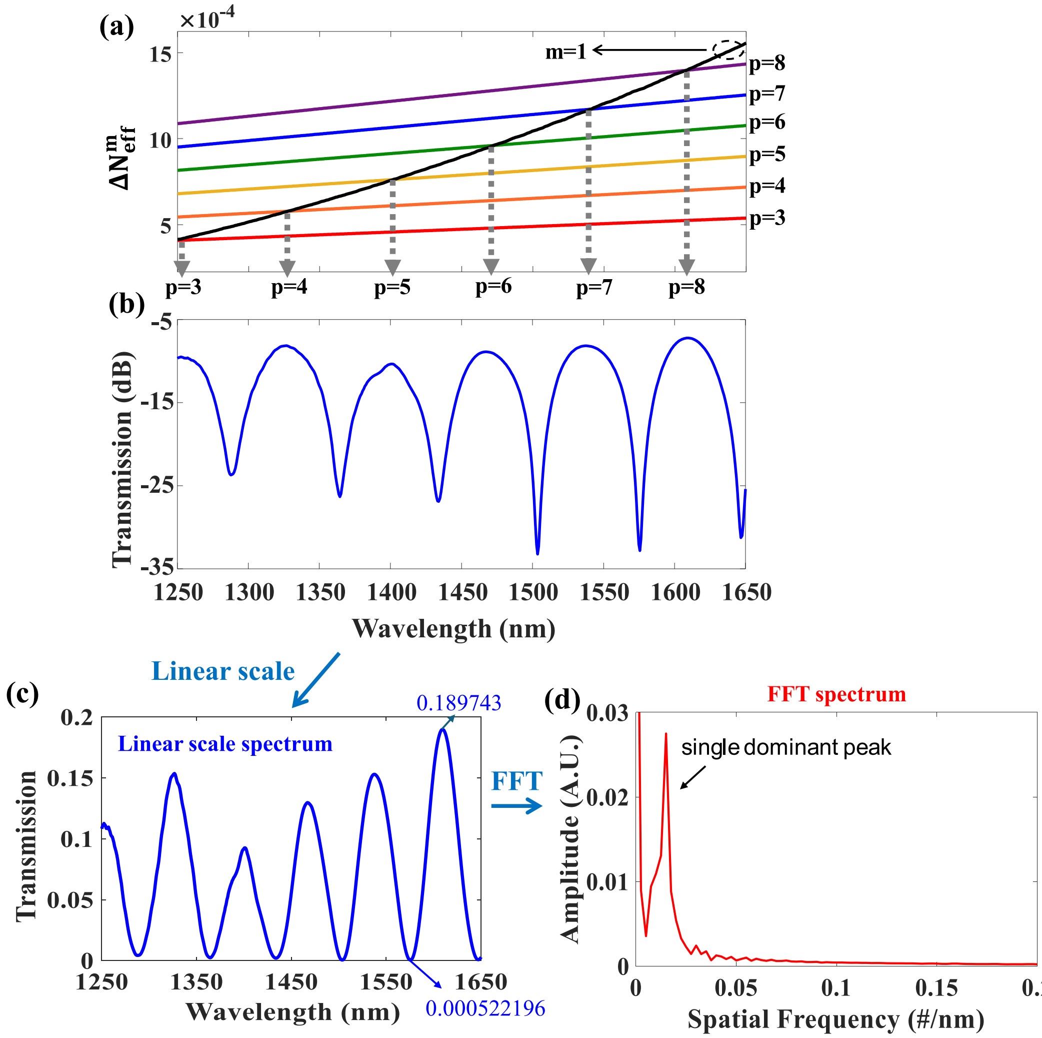

Fig. 3. Comparison of theoretically calculated peaks and experimental results. (a) The relationship between $\Delta N_{eff}^{m=1}$(black line) and $\frac{p\times\lambda_{max}^{m}}{L}$ with p = 3–8 interference orders (rainbow-colored lines). (b) The experimental interference spectrum of the proposed LCFMZI was measured by OSA. (c) Linear scale interference spectrum. (d) FFT Spectrum analysis of the interference spectrum.

range of the 3rd–8th interference orders. The theoretical and experimental results agree perfectly with the results of Fig. 3(a) and 3(b).

Moreover, to further analyze the interference performance, spectral interference's visibility and mode coupling are investigated. Fig. 3(c) presents the interference spectrum of the LCFMZI converted from a logarithmic (dB) to a linear scale. This transformation is essential for accurately evaluating interference visibility and extracting meaningful spectral characteristics. From the results of Fig. 3(c), the best interference visibility can be obtained as follows: $V = \frac{I_{max}-I_{min}}{I_{max}+I_{min}} = \frac{0.189743-0.000522196}{0.189743+0.000522196} = 0.9945 = 99.45\ \%$. Here, I_{max} and I_{min} are maximum and minimum transmission, respectively. Based on the visibility evaluation, the highest visibility reaches 99.45 %, demonstrating the strong interference characteristics of the proposed device. A Fast Fourier Transform (FFT) of the interference spectrum is also performed to extract the dominant spatial frequency, as displayed in Fig. 3(d). The resulting FFT spectrum exhibits a single dominant peak and indicates the interference pattern is highly periodic which demonstrates that the interference pattern is primarily governed by two-mode interference.

Based on the above analysis in Fig. 3, the two-mode interference mechanism in this device can be attributed to the interference between the core mode and the first-order cladding mode. Once the proposed LCFMZI absorbs the laser light and is heated, the temperature-dependent refractive index variation varies the optical path difference (OPD) between these two modes, leading to a shift in the interference spectrum. The OPD and T variation can be expressed as follows:

$$\frac{d(OPD)}{dT} = L\cdot\left(\alpha_{co} - \alpha_{cl,m} + \frac{\partial\left(\Delta N_{eff}^{m}\right)}{\partial\lambda}\frac{d\lambda}{dT}\right) \tag{4}$$

Here, $\alpha_{co} = \frac{dN_{eff}^{co}}{dT}$ *and* $\alpha_{cl,m} = \frac{dN_{eff}^{cl,m}}{dT}$ Are the thermal dependence of the effective refractive indices for the liquid core and cladding are given by their thermos optic coefficients.

The effective refractive index difference ΔN_{eff}^{m} is a function of wavelength (as shown in the black line of Fig. 3(a)) and varies with λ. Based on Eq. (4), the optical path difference (OPD) of the proposed LCFMZI device can be effectively tuned by selecting liquids with different thermo-optic coefficients (α_{co}) and refractive index dispersion ($\frac{\partial\left(\Delta N_{eff}^{m}\right)}{\partial\lambda}$) characteristics. This flexibility makes the developed device highly adaptable for various applications.

3. Experimental results and discussion

The experiment was performed to evaluate the effectiveness of the slight light absorption process by the filled liquid in the proposed liquid core fiber Mach–Zehnder interferometer (LCFMZI). A laser diode with a wavelength of 980 nm, typically used to pump an erbium-doped fiber, is coupled with a broadband light source (BLS) into the proposed fiber device via wavelength division multiplexing (WDM). The experiment's ambient temperature was strictly maintained at 25 °C to ensure thermal stability, allowing the device to be isolated from external conditions and focus solely on the laser heating effect. The packaged fiber device was placed in a thermally insulated chamber to eliminate external thermal influences of the surroundings, minimizing heat transfer via conduction, convection, and radiation. Although the 980 nm LD can provide over 100 mW of output, significant temperature changes occur with less than 1 mW of light power. To better understand the absorption of the weak power of the LCFMZI, we fusion spliced about 1.2 m of optical communication commercial fiber, SMF 28 as an attenuation section to enhance the loss of the LD power, as shown in Fig. 4. The experimental setup for the measurement, illustrates Fig. 4. Here, the BLS with wavelengths of 1250 ~ 1650 nm is incident. An optical spectrum analyzer (OSA) is used to measure the variations of interference spectra by the slight light influence.

The setup indicates that the SMF-28 can decrease the incident light of 980 nm into the LCFMZI. The red line of Fig. 5(a) displays the Light-Current (LI) curve measurement of the 980 nm LD as it was ready to enter into the fiber device (point A in Fig. 4). The blue line is according to information from the official website of @Cargille lab to have the information of the filled liquid with a length of 1 cm can have about 5 % absorption of light with wavelength 980 nm [19]. The blue line in Fig. 5 (a) plots the light power that the liquid core would absorb. The liquid's absorbance was further analyzed using UV–VIS spectroscopy to evaluate its light absorption properties. The absorbance (A) is calculated using the relation $A = -\log_{10}(T_r)$, where T_r represents the transmittance of the liquid sample with a length of around 0.92 cm, as shown in Fig. 5(b). Based on the results in Fig. 5(b), the absorbance of approximately 0.04 corresponds to a transmittance T_r of around 0.912. This confirms that the filled optical liquid, with a refractive index of $n_D = 1.46$, exhibits minimal absorption at a wavelength of 980 nm.

To verify the light absorption of the LCFMZI, we vary the driven current (I_d) of the 980 nm-LD to control the light power. As the liquid core absorbs the light power, it can be heated, and its RI is reduced due to the TOC being negative. In this condition, the effective index of the core mode is modulated significantly to change the optical path difference of the interference of the LCFMZI. Fig. 6 shows the experimental results of the device when the driven current of LD from 0–70 mA with an interval of 2 mA to evaluate the slight light absorbing effect on the obvious variation transmission spectra. Due to the threshold current (I_{th}) of the used LD around 38 mA, the interference spectrum shows nearly fixed when the driven current I_d is below 38 mA, as illustrated in Fig. 6 (a). While the I_d approaches the threshold current, the interference spectra significantly shift to a longer wavelength (redshifted), displayed in Fig. 6(b) and Fig. 6(c). We monitor one wavelength dip within the range of around 1480 nm–1640 nm to determine the optical responses by the 980 nm light absorption. Fig. 6(d) shows the wavelength shift over 124 nm can be achieved with an absorption power of merely 0.566 mW. The sensitivity of + 219.08 nm/mW and 3.647 nm/mA with the linear response ($r^2 = 0.9993$) is obtained. The unique characteristics of the wavelength redshifted can be realized by the thermal effect on the liquid increasing its T to reduce the RI and N_{eff}^{co}, as well as lowering the *effectiveindexdifference*ΔN_{eff}^{m}. In the experimental results, the thermal optics coefficient (TOC) of the Cargille-liquid ($n_D = 1.46$) in liquid core with -3.89×10^{-4} °C^{-1} is much higher than that of silica fiber ($+8.6 \times 10^{-6}$ °C^{-1}). It has negative characteristics, resulting in highly ultra-high sensitivity to the device.

It is worth mentioning that the RI of the liquid core reduces by absorbing the laser light. It gets smaller and has lower values than the original black line in Fig. 3(a). In this condition, the intersection points of the curve with each interference order (p) of peaks will move to longer wavelengths (redshifted). Fig. 6(e) plots the estimation of the curve (red line) of effective index *difference*ΔN_{eff}^{m} heated by the 980 nm light. We can understand that with the same order p, the intersection points of the red line are located at longer wavelengths to verify redshifts of the optical spectra.

To ensure the effectiveness of the experimental design for liquid filling with the oblique gap and light absorption by the liquid core, we conducted a thorough study of the real-time capillary action in the HCF structure. The 1550 nm laser is coupled into the fiber device, and the measurement results by an oscilloscope are plotted in Fig. 7(a), showing that the liquid fully fills the HCF core in approximately 5.31 s. A noticeable noise is observed in the measurement, particularly before the liquid fills the core of HCF. This is likely caused by the significant refractive index discontinuity between the tilted fiber gap and the HCF, leading to more substantial optical perturbations. As the liquid gradually fills into the HCF, the signal perturbations diminish and eventually stabilize. In another experiment, we evaluated the transient responses of the proposed LCFMZI affected by the 980 nm laser light. The signal light was launched into the LCFMZI, and its response was detected and measured by an oscilloscope. The 980 nm LD "off" and "on" switch alternates every cycle, and the corresponding responses are shown in Fig. 7(b). It takes only ~ 2.91 s to rise to the steady state of power absorption at the first cycle. Subsequently, LD is turned off so that the measured power returns to the initial state at the beginning, and the dropping response time is longer ~ 9.95 s. The second cycle of laser turn on and off indicates the responses of 3.58 s and 12.08 s for the rise and fall times, respectively. The transient responses of the proposed LCFMZI affected by the LD switching can achieve the rise and fall times averages of 3.25 s and 11.01 s, respectively. As the liquid absorbs the 980 nm laser light, it converts the absorbed light into thermal energy, causing its T to rise. When the laser is turned off, the liquid's heat needs to dissipate,

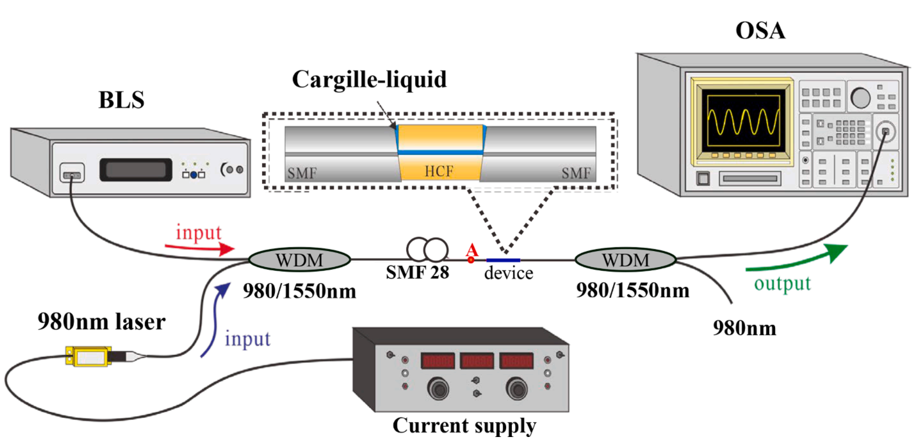

Fig. 4. Experimental setup for measuring the LCFMZI affected by 980 nm light absorption.

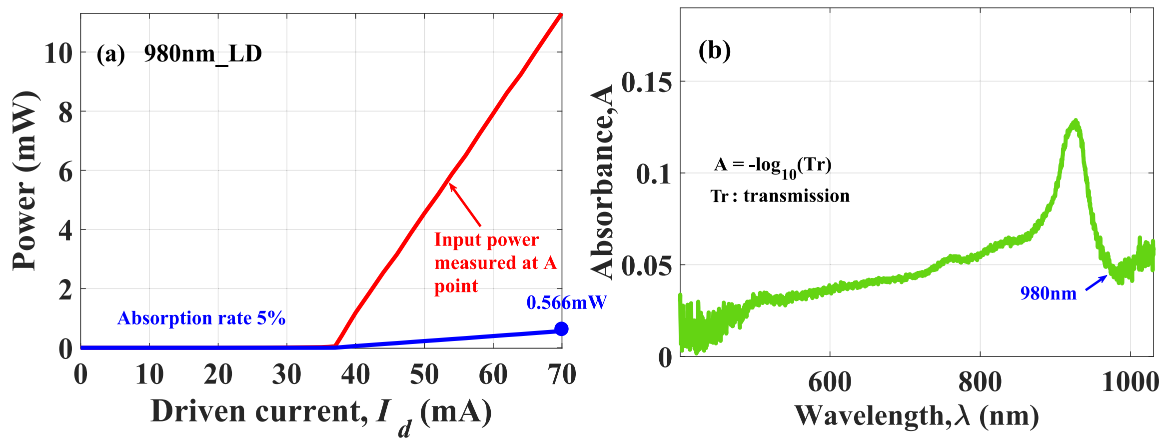

Fig. 5. (a) LI curve of the 980 nm LD measured at A point (red line) and the estimated light power absorbed by the filled liquid core (blue line). (b) The absorbance of the filled liquid was measured by UV–VIS spectroscopy.

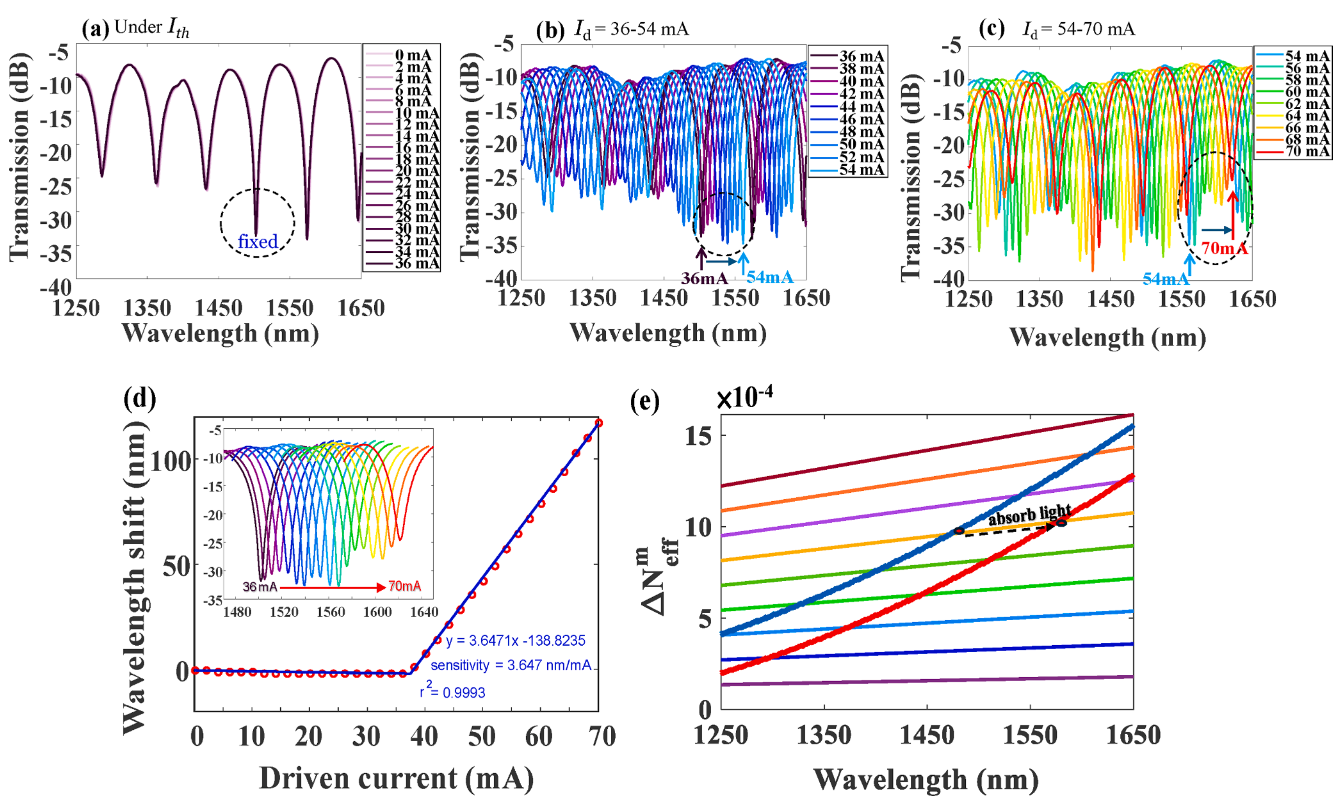

Fig. 6. (a)-(c) Transmission spectra with I_d of 980 nm LD from 0 mA–70 mA. (d) Wavelength shifts versus I_d for the determined sensitivity. Insects show corresponding spectra with increasing I_d . (e) ΔN^m_{eff} curve (red line) heated by the light.

primarily through conduction, convection, or radiation. If the environment around the liquid has poor thermal conductivity or limited heat dissipation mechanisms, the heat loss rate will be slower, leading to a longer fall time.

Furthermore, it can be realized that during the cooling process, the liquid's T decreases more slowly to return to its initial state, which extends the fall time. We have successfully developed an ultrahigh-sensitivity liquid-core fiber interferometer. This advanced device offers flexibility in selecting appropriate filling materials tailored to specific sensing applications across diverse fields. Materials with high thermo-optic coefficients (TOC) or unique optical anisotropic properties can be utilized. Moreover, this device enables light-controlled modulation of the optical spectrum, further emphasizing its significant potential for high-value applications.

4. Conclusion

This study successfully demonstrates a novel liquid-core fiber Mach–Zehnder interferometer (LCFMZI) that takes advantage of the low light absorption of the liquid core to achieve ultrasensitive spectral responses. The device utilizes a liquid core filled with Cargille liquid (n_D = 1.46) featuring a high thermo-optic coefficient (TOC) of $-3.89 \times 10^{-4}\ ^{\circ}C^{-1}$ and inherent absorption at a wavelength of 980 nm. The little absorption of the 980 nm laser diode (LD) induces a localized T increase, resulting in a reduction in the liquid's refractive index (RI) and a corresponding reduction in the optical path difference within the LCFMZI. This mechanism produces a significant wavelength shift in the interference pattern. Experimental results confirm remarkable spectral shifts of 124 nm across a broadband wavelength range of 1250–1650 nm with

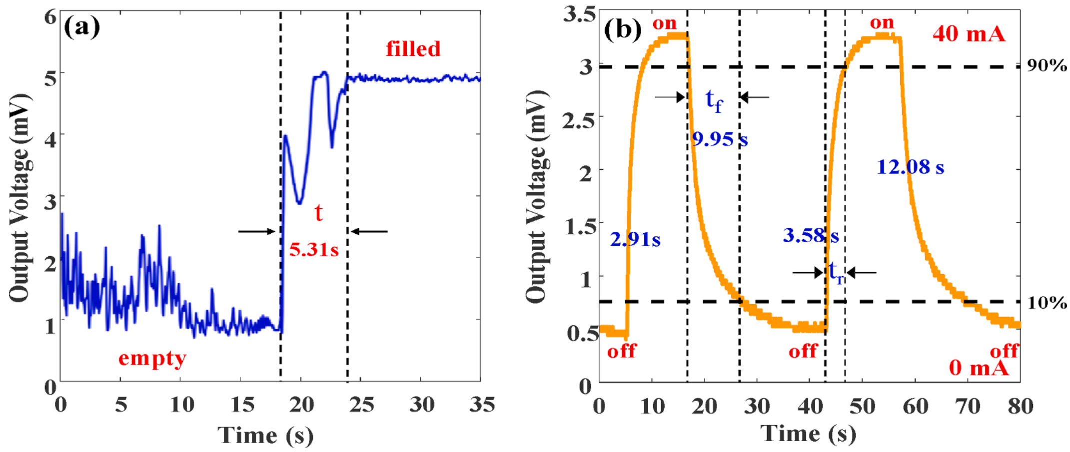

Fig. 7. (a) Dynamic response of filling process with Cargill-liquid (n_D = 1.46) into the core of the HCF. (b) Transient responses of the LCFMZI with successive laser cycles on and off.

absorbing power as low as 0.566 mW, validating the LCFMZI's ultrahigh sensitivity. It achieves an impressive + 219.08 nm/mW and 3.647 nm/mA with excellent linearity. The transient response analysis reveals rise and fall times averaging 3.25 s and 11.01 s, respectively, under the influence of the laser light. Moreover, the developed device provides remarkable flexibility in selecting appropriate filling materials for various sensing applications. It allows using materials with high TOC, notable absorbance (A), or unique optical anisotropic properties, enabling precise light-controlled modulation of the optical spectrum.

CRediT authorship contribution statement

Cheng-Ling Lee: Writing – review & editing, Writing – original draft, Validation, Supervision, Resources, Project administration, Methodology, Investigation, Funding acquisition, Formal analysis, Conceptualization. **Jen-Te Chao:** Software, Methodology, Data curation. **Ying-Zhen Huang:** Visualization, Software. **Yi-Hua Wu:** Data curation. **Yi-Kai Chiu:** Data curation. **Wei-Wei Hsiang:** Methodology, Investigation.

Declaration of competing interest

The authors declare that they have no known competing financial interests or personal relationships that could have appeared to influence the work reported in this paper.

Acknowledgment

This research was funded by theNational Science and Technology Council Taiwan, NSTC 110-2221-E-239 -025 -MY2 and NSTC 113-2221-E-239-016.

Data availability

The data that has been used is confidential.

References

[1] D. W. Duan, Y. J. Rao, L. C. Xu, T. Zhu, D. Wu, Yao, In-fiber Mach–Zehnder interferometer formed by large lateral offset fusion splicing for gases refractive index measurement with high sensitivity, Sensors and Actuators B: Chemical, 160 (1) J. (2011) 1198-1202. Doi: 10.1016/j.snb.2011.09.048.
[2] Z. Tian, S.S. Yam, H.P. Loock, Single-mode fiber refractive index sensor based on core-offset attenuators, IEEE Photon. Technol. Lett. 20 (16) (2008) 1387–1389, https://doi.org/10.1109/LPT.2008.926832.
[3] D.W. Duan, Y.J. Rao, L.C. Xu, T. Zhu, M. Deng, D. Wu, J. Yao, In-fiber Fabry–Perot and Mach–Zehnder interferometers based on hollow optical fiber fabricated by arc fusion splicing with small lateral offsets, Opt. Commun. 284 (22) (2011) 5311–5314, https://doi.org/10.1016/j.optcom.2011.07.052.
[4] T.H. Xia, A.P. Zhang, B. Gu, J.J. Zhu, Fiber-optic refractive-index sensors based on transmissive and reflective thin-core fiber modal interferometers, Opt. Commun. 283 (10) (2010) 2136–2139, https://doi.org/10.1016/j.optcom.2010.01.031.
[5] X. Huang, X. Li, J. Yang, C. Tao, X. Guo, H. Bao, Y. Zhu, et al., An in-line Mach-Zehnder interferometer using thin-core fiber for ammonia gas sensing with high sensitivity, Sci. Rep. 7 (1) (2017) 44994, https://doi.org/10.1038/srep44994.
[6] Y. Li, L. Wang, Y. Chen, D. Yi, F. Teng, X. Hong, D. Luo, et al., High-performance fiber sensor via Mach-Zehnder interferometer based on immersing exposed-core microstructure fiber in oriented liquid crystals, Opt. Express 28 (3) (2020) 3576–3586, https://doi.org/10.1364/OE.385521.
[7] H. Zhang, S. Gao, Y. Luo, Z. Chen, S. Xiong, L. Wan, Z. Li, et al., Ultrasensitive Mach-Zehnder interferometric temperature sensor based on liquid-filled D-shaped fiber cavity, Sensors 18 (4) (2018) 1239, https://doi.org/10.3390/s18041239.
[8] S. Liu, H. Zhang, L. Li, L. Xiong, P. Shum, Liquid Core Fiber Interferometer for Simultaneous Measurement of Refractive Index and Temperature, IEEE Photon. Technol. Lett. 31 (2) (2019) 189–192, https://doi.org/10.1109/LPT.2018.2889753.
[9] S. Gao, W. Zhang, H. Zhang, C. Zhang, Reconfigurable and ultra-sensitive in-line Mach-Zehnder interferometer based on the fusion of microfiber and microfluid, Appl. Phys. Lett. 106 (8) (2015) 084103, https://doi.org/10.1063/1.4913921.
[10] H. Liu, H. Zhang, Y. Miao, B. Liu, Y. Li, X. Zhao, L. Lin, A light-intensity-controlled microfiber-assisted Mach–Zehnder interferometer based on ethyl orange solution under 532 nm laser excitation, Sens. Actuators B 216 (2015) 229–234, https://doi.org/10.1016/j.snb.2015.04.051.
[11] L. Zhao, L. Jiang, S. Wang, H. Xiao, Y. Lu, H.L. Tsai, A high-quality Mach-Zehnder interferometer fiber sensor by femtosecond laser one-step processing, Sensors 11 (1) (2010) 54–61, https://doi.org/10.3390/s110100054.
[12] M. Deng, L. Liu, Y. Zhao, G. Yin, T. Zhu, Highly sensitive temperature sensor based on an ultra-compact Mach–Zehnder interferometer with side-opened channels, Opt. Lett. 42 (18) (2017) 3549–3552, https://doi.org/10.1364/OL.42.003549.
[13] J. Luo, S. Liu, Y. Zhao, Y. Chen, K. Yang, K. Guo, Y. Wang, et al., Phase-shifted fiber Bragg grating modulated by a hollow cavity for measuring gas pressure, Opt. Lett. 45 (2) (2020) 507–510, https://doi.org/10.1364/OL.381452.
[14] C.L. Lee, C.T. Ma, K.C. Yeh, Y.M. Chen, A Dual-Cavity Fiber Fabry–Pérot Interferometer for Simultaneous Measurement of Thermo-Optic and Thermal Expansion Coefficients of a Polymer, Polymers 14 (22) (2022) 4966, https://doi.org/10.3390/polym14224966.
[15] H. Liang, W. Zhang, H. Wang, P. Geng, S. Zhang, S. Gao, J. Li, et al., Fiber in-line Mach-Zehnder interferometer based on near-elliptical core photonic crystal fiber for temperature and strain sensing, Opt. Lett. 38 (20) (2013) 4019–4022, https://doi.org/10.1364/OL.38.004019.
[16] J. Zhou, Y. Sun, H. Liu, H. Li, Y. Wang, J. Jiang, J. Yao, The Highly Sensitive Refractive Index Sensing of Seawater Based on a Large Lateral Offset Mach–Zehnder Interferometer, *Sensors* 24 (12) (2024) 3887, https://doi.org/10.3390/s24123887.
[17] J. Yang, M. Yang, C.Y. Guan, J.H. Shi, Z. Zhu, P. Li, L.B. Yuan, et al., In-fiber Mach-Zehnder interferometer with piecewise interference spectrum based on hole-assisted dual-core fiber for refractive index sensing, *Opt. Express* 26 (15) (2018) 19091–19099, https://doi.org/10.1364/OE.26.019091.
[18] C.L. Lee, W.R. Zhuo, T.K. Liu, Highly Modulated In-Fiber Mach–Zehnder Interferometer Based on an Ultracompact Leaky-Guided Liquid Core, Sensors 22 (3) (2022) 808, https://doi.org/10.3390/s22030808.
[19] https://www.cargille.com/refractive-index-liquids/.

[20] H. Jeong, K. Oh, Theoretical analysis of cladding-mode waveguide dispersion and its effects on the spectra of long-period fiber grating, J. Lightwave Technol. 21 (8) (2003) 1838. https://opg.optica.org/jlt/abstract.cfm?URI=jlt-21-8-1838.

[21] B.H. Lee, Y. Liu, S.B. Lee, S.S. Choi, J.N. Jang, Displacements of the resonant peaks of a long-period fiber grating induced by a change of ambient refractive index, Opt. Lett. 22 (23) (1997) 1769–1771, https://doi.org/10.1364/OL.22.001769.

[22] Okamoto Katsunari. (2006) Fundamentals of optical waveguides (2nd ed.) Academic Press.